Improvement in Electrochemical Performance of Lithium Rich Li_2RuO_3 Cathode With co-doping Strategy

C. Bapanayya[1,2] * G. Giribabu[3], G. Srinu[2], R.P. Vijayalakshmi[1]
[1]*Department of Physics, S.V. University, Tirupati-517001, Andhra Pradesh, India*
[2]*Department of Physics, S.V.A. Govt. College, Srikalahasti-517644, Andhra Pradesh, India*
[3]*Government Degree College, Eluru – 534001, Andhra Pradesh, India*
**Correspondence address: bapustf@gmail.com*

Abstract

Lithium-rich layered oxides based on Ru are interesting as cathode materials because they have high energy density and reversible capacity. However, due to the problems of weak structural stability and voltage decay, their commercial utility is limited. To address this, we use a DFT+U quantum mechanics to investigate the co-doping strategy on Li_2RuO_3 (LRO) for improved battery performance. In particular, the effect of two co-dopants Ti and Co has been studied. The co-doping strategy has been found to significantly improve the structural and thermal stability of LRO. By slowing the oxygen removal reaction, Ti and Co improve structural stability. Co-doping with Ti and Co increases the maximum open circuit voltage at least by 5.5% and decreases the voltage reduction by a minimum of 44%. Bandgap is also increased by a minimum of 6% with co-doping. In particular, $Li_2Ru_{0.5}Ti_{0.375}Co_{0.125}O_3$ provides the highest maximum voltage of 4.4V with 61% decrease in the voltage reduction and 40% lower bandgap (0.45eV).

Key words: Li_2RuO_3, Co-doping strategy, DFT+U, Li-ion battery cathode

1. Introduction

As a portable source of energy, lithium-ion batteries, often known as LIBs, are becoming more popular in electronic devices [1]. As a result of the increasing importance of battery technology, there is a rising need for LIBs with improved electrochemical performance [2–4]. Electric vehicles (EVs) and hybrid electric vehicles (HEVs) demand more sophisticated LIBs [5,6] with improved electrochemical characteristics due to disadvantages such as capacity loss and poor energy density of commercially available cathode materials such as $LiNi_xMn_yCo_{1-x-y}O_2$, $LiFePO_4$, and $LiCoO_2$ [7–9]. Therefore, many researchers have concentrated on identifying the best suitable cathode material. Due to better energy density and capacity retention, Lithium-rich layered oxide (LLO) cathodes, specifically Li_2MO_3 (where M is a transition metal), have emerged as the most promising cathode materials [10]. Li_2MO_3 consists of more Li ions for intercalation and deintercalation, which results in increased reversible discharge capacity (e.g., for Li_2MnO_3 discharge capacity is 460 $mAhg^{-1}$) [10]. The increased energy density of Li_2MO_3 cathodes is due to the cumulative anionic and cationic redox reactions which result in increased capacity. The charge compensation in anionic and cationic redox reactions is due to the participation of products of oxygen extraction reaction at higher voltages [11].

However, in Li_2MO_3 cathode materials, the first cycle of the redox reaction is irreversible, which results in a significant release of oxygen [12]. Furthermore, during the intercalation and deintercalation processes, a spinel-like structure is formed in the internal phase which causes the decrease in the intrinsic voltage and capacity [13–15]. Recent studies

have shown that Li_2RuO_3 (LRO) cathode material, which has a monoclinic C2/c layered structure, perform better in terms of the reversibility of the oxygen extraction process during charge-discharge cycles [16,17]. In addition, the cation ordering and crystal structure of this cathode material could influence its electrochemical performance due to variations in O-Li-O bond formations and Li-ion diffusion paths. Recent studies have shown that doping this cathode material further improves electrochemical properties. For example, Arunkumar et al. [18] reported that adding aliovalent Co^{3+} to the Lithium rich Li_2RuO_3 improves the structural stability and reversibility of the cathode due to high cation ordering. Using first-principles calculations on Li_2RuO_3, Zheng et al. [17] studied the effect of Ni substitution on the oxygen redox process. They discovered that Ni dopants considerably reduce the oxygen oxidation reaction, resulting in an increase in capacity. In another study, Kalathil et al. [19] reported that doping with Ti enhances structural stability, Li-in diffusion and electronic conductivity. Lithium-ion battery electrodes doped with Mg [20–22], Ni [23,24], Co [25–29], and N [30,31] have been shown to improve electrochemical performance in similar studies. In addition, a co-doping technique on Li_2RuO_3 using Na and Cr elements was investigated by Tian et al. [32]. They reported that doping with Cr boosts capacity, while doping with Na reduces voltage decay. More recently, Moradi et al. [33,34] have reported that co-doping of Tc, Rh, and Pd with Ti in pristine Li_2RuO_3 reduces the oxygen removal from the cathodes, improves maximum open circuit voltage, structural and thermodynamic stability.

In this work, we study the effect of co-doping with Ti and Co as co-dopants on the electrochemical performance of Li_2RuO_3. The elements Ti and Co were chosen as co-dopants because they have comparable atomic radii with Ru and these elements when doped separately were found to improve the structural stability, reversibility, electrical conductivity and theoretical capacity of pristine Li_2RuO_3 [18,35]. In this study we employed the DFT+U quantum mechanical calculations to compute effective parameters that enhances the electrochemical performance of the pristine Li_2RuO_3 cathode.

2. Computational Methods

Li_2RuO_3 is a layered oxide with a high lithium content. It has a stable monoclinic structure (space group: C2/c, No. 15). Figure 1 shows a single unit cell of pristine Li_2RuO_3 containing 48 atoms of Li, Ru, and O. Co-doped cathode materials were obtained by substituting one half of the Ru atoms with the Ti and Co elements. Quantum mechanical calculations were performed on pristine Li_2RuO_3 and co-doped cathode materials within density functional theory (DFT). The DFT+U method, which involves utilising the DFT approximation to calculate energies while considering Hubbard U [36] values for the transition metals in the system and PBE (Perdew–Burke–Ernzerhof) [37] (PBE+U) as the exchange-correlation function, is more accurate than the DFT method when transition metals are involved [10,38]. Therefore, the DFT+U with PBE+U has been used for all calculations in this work. The Hubbard U values for different transition metals which were used to rectify the significant correlation of d-orbitals in transition metal ions are given in Table 1.

Table 1: Hubbard U- values of transition metals used in this study [39–41]

Transition Metal	Hubbard U-value
Ru	2.0
Ti	2.5
Co	3.0

The experimental data by James et al. [42], was used to determine the initial lattice parameters and atomic locations of Li_2RuO_3. A supercell of size $2 \times 2 \times 2$ containing 48 atoms in each cell was used to represent the periodic crystal and all calculations were carried out on this supercell. In all calculations, the plane wave cut-off energy was fixed at 500eV and energy convergence requirement was fixed at 10^{-4} eV/atom. In order to obtain the energetically favourable geometry, all atoms in the unit cell were completely relaxed. Subsequently, the co-doped cathodes were obtained by substituting one half of Ru atoms with Ti and Co elements. In order to investigate the structural changes upon doping, X-ray powder diffraction (XRD) technique was used. The powder XRD patterns of the cathodes were simulated using VESTA-3 visualization tool [43]. The source of X-ray radiation was monochromatic Cu-K_α of wavelength 1.54059Å. Table 2 shows the weight percentage analysis of various elements present in the undoped and co-doped cathodes.

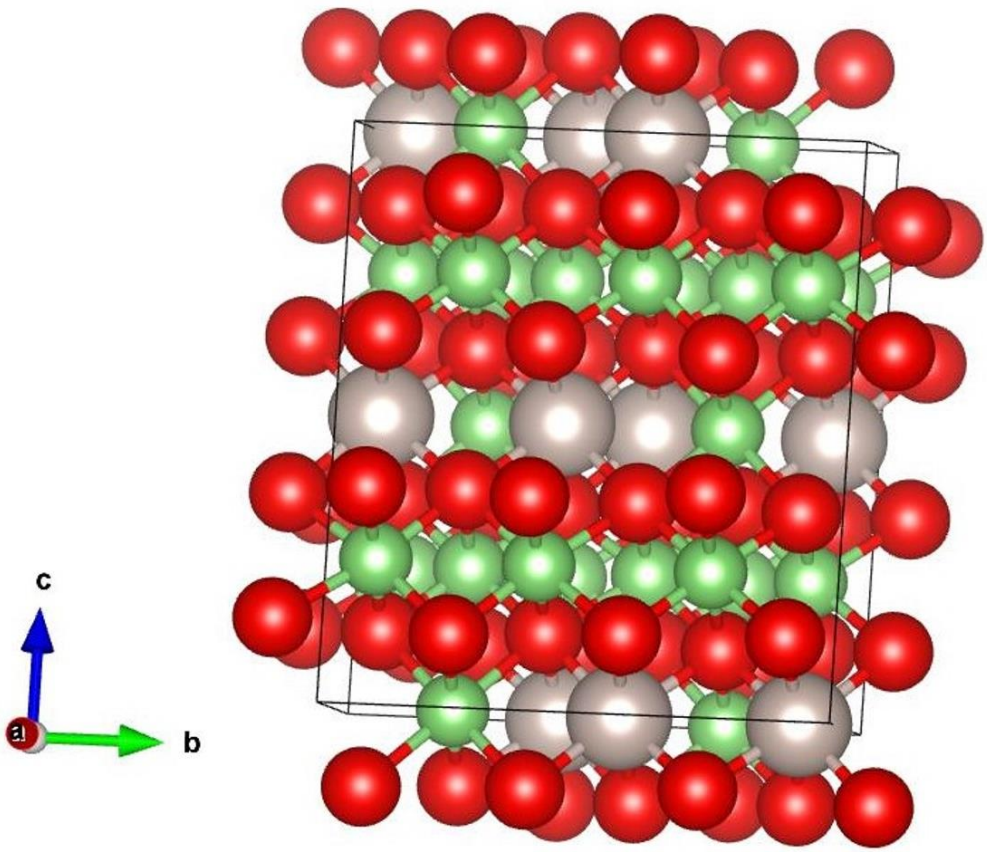

Figure 1: Single unit cell of pristine Li_2RuO_3 containing 48 atoms.

Table 2: Weight percentages of elements within the cathode materials

Cathode	**Weight percentage**				
	Li	**Ru**	**Ti**	**Co**	**O**
Li_2RuO_3	8.52	62.03	0.00	0.00	29.46
$Li_2Ru_{0.5}Ti_{0.5}Co_0O_3$	10.18	37.06	17.55	0.00	35.2

$Li_2Ru_{0.5}Ti_{0.375}Co_{0.125}O_3$	10.08	36.69	13.03	5.35	34.85
$Li_2Ru_{0.5}Ti_{0.25}Co_{0.25}O_3$	9.98	36.33	8.6	10.59	34.5
$Li_2Ru_{0.5}Ti_{0.125}Co_{0.375}O_3$	9.88	35.97	4.26	15.73	34.16
$Li_2Ru_{0.5}Ti_0Co_{0.5}O_3$	9.78	35.62	0.00	20.77	33.83

3. Results and Discussion

3.1. Theoretical Capacity

The theoretical charge capacity of a cathode is obtained from the following relation [44]:

$$Q_{theo} = \frac{nF}{3.6 \times MW} \quad (1)$$

where, *n* is the number of moles of Li present in the cathode, *F* is the Faraday constant, and MW is the molecular weight of the cathode. For all the studied cathodes, the value of *n* is 2.

Table 3: Theoretical charge capacities and percentage change of co-doped cathodes and pristine Li_2RuO_3

Cathode	$Q_{theoretical}$ **(**$mAhg^{-1}$**) (percentage change)**
Li_2RuO_3	329.0
$Li_2Ru_{0.5}Ti_{0.5}Co_0O_3$	393.2 (19.5%)
$Li_2Ru_{0.5}Ti_{0.375}Co_{0.125}O_3$	389.1 (18.3%)
$Li_2Ru_{0.5}Ti_{0.25}Co_{0.25}O_3$	385.4 (17.1%)
$Li_2Ru_{0.5}Ti_{0.125}Co_{0.375}O_3$	381.6 (16%)
$Li_2Ru_{0.5}Ti_0Co_{0.5}O_3$	377.9 (14.9%)

The calculated theoretical capacities of the cathodes under study are presented in Table 3. It can be seen from Table 3, that the theoretical charge capacities of the co-doped cathodes are higher than that of the parent LRO cathode. More precisely, $Li_2Ru_{0.5}Ti_{0.5}Co_0O_3$, $Li_2Ru_{0.5}Ti_{0.375}Co_{0.125}O_3$, $Li_2Ru_{0.5}Ti_{0.25}Co_{0.25}O_3$, $Li_2Ru_{0.5}Ti_{0.125}Co_{0.375}O_3$, and $Li_2Ru_{0.5}Ti_0Co_{0.5}O_3$ have 19.5%, 18.3%, 17.1%, 16%, and 14% respectively, higher capacity than LRO. Further, among the studied cathodes, $Li_2Ru_{0.5}Ti_{0.5}Co_0O_3$ has the highest theoretical capacity. In terms of theoretical charge capacity ($Q_{theoretical}$), the decreasing order of the cathodes is:

$Li_2Ru_{0.5}Ti_{0.5}Co_0O_3 > Li_2Ru_{0.5}Ti_{0.375}Co_{0.125}O_3 > Li_2Ru_{0.5}Ti_{0.25}Co_{0.25}O_3 > Li_2Ru_{0.5}Ti_{0.125}Co_{0.375}O_3 > Li_2Ru_{0.5}Ti_0Co_{0.5}O_3 > Li_2RuO_3$

3.2. Formation Energy (FE)

Formation Energy (FE) is the amount of energy necessary to construct a cathode from its constituent elements in their standard states. The stability of the cathode material depends on the formation energy FE in such a way that if the formation energy more negative, the stability of the cathode is more.

The formation energy of the studied cathodes is calculated using the formula:

$$FE = E\left[Li_2Ru_{0.5}Ti_yCo_{05-y}O_3\right] - 2E[Li] - 0.5E[Ru] - yE[Ti] - (0.5-y)E[Co] - \frac{3}{2}E[O_2] \quad (2)$$

where, FE is the formation energy of the cathode, $E\left[Li_2Ru_{0.5}Ti_yCo_{05-y}O_3\right]$ is the computed total energy of $Li_2Ru_{0.5}Ti_yCo_{05-y}O_3$ after geometry optimization, $E[Li], E[Ru], E[Ti], E[Co]$, and $E[O_2]$ are respectively the total energies of Li, Ru, Ti, Co and O in their standard states.

Table 4: Formation energy values and percentage change of cathodes for different doping combinations calculated using the quantum mechanical methods

Cathode	Formation Energy (eV) (percentage change)
Li_2RuO_3	-11.75
$Li_2Ru_{0.5}Ti_{0.5}Co_0O_3$	-13.94 (18.6%)
$Li_2Ru_{0.5}Ti_{0.375}Co_{0.125}O_3$	-14.81 (26%)
$Li_2Ru_{0.5}Ti_{0.25}Co_{0.25}O_3$	-14.50 (23.4%)
$Li_2Ru_{0.5}Ti_{0.125}Co_{0.375}O_3$	-14.23 (21.1%)
$Li_2Ru_{0.5}Ti_0Co_{0.5}O_3$	-13.91 (18.4%)

From Table 4 it can be seen that, FE of all cathodes is negative, indicating that the cathodes under study have stable crystal structures. Further, the FE of each co-doped cathode is higher than that of the parent LRO cathode. More precisely, the formation energies of $Li_2Ru_{0.5}Ti_{0.5}Co_0O_3$, $Li_2Ru_{0.5}Ti_{0.375}Co_{0.125}O_3$, $Li_2Ru_{0.5}Ti_{0.25}Co_{0.25}O_3$, $Li_2Ru_{0.5}Ti_{0.125}Co_{0.375}O_3$, and $Li_2Ru_{0.5}Ti_0Co_{0.5}O_3$ are respectively 18.6%, 26%, 23.4%, 21.1%, and 18.4% higher than that of the parent LRO cathode. In other words, the co-doping with Ti and Co increases the formation energy and hence the structural stability of the cathode. Among all the studied cathodes, $Li_2Ru_{0.5}Ti_{0.375}Co_{0.125}O_3$ is the most stable cathode because it has the highest formation energy. Based on the FE values, the order of stability of cathodes is:

$Li_2Ru_{0.5}Ti_{0.375}Co_{0.125}O_3$ > $Li_2Ru_{0.5}Ti_{0.25}Co_{0.25}O_3$ > $Li_2Ru_{0.5}Ti_{0.125}Co_{0.375}O_3$ > $Li_2Ru_{0.5}Ti_{0.5}Co_0O_3$ > $Li_2Ru_{0.5}Ti_0Co_{0.5}O_3$ > Li_2RuO_3

3.3. Powder X-ray diffraction (XRD)

In this study, a significant proportion (50%) of the Ruthenium (Ru) sites in LRO cathode have been substituted with Ti and Co atoms to obtain co-doped cathodes. As a result, all the cathodes have been investigated for consequent structural changes due to a high proportion of dopants by comparing their XRD patterns. Upon completion of the geometry optimization of the cathodes, the powder XRD patterns were calculated and presented in Figure 2 along with the experimental data of the LRO cathode. As seen in the Figure 2, the XRD patterns of the studied cathodes are in good agreement with the experimental data of LRO cathode. Specifically, the Bragg angles of the studied cathodes and the peak positions obtained from the experimental data are very close to each other, which indicates that a high percentage of doping with transition metals Ti and Co will not lead to any appreciable structural changes. In other words, the crystal structure remains stable upon doping with the Ti and Co atoms.

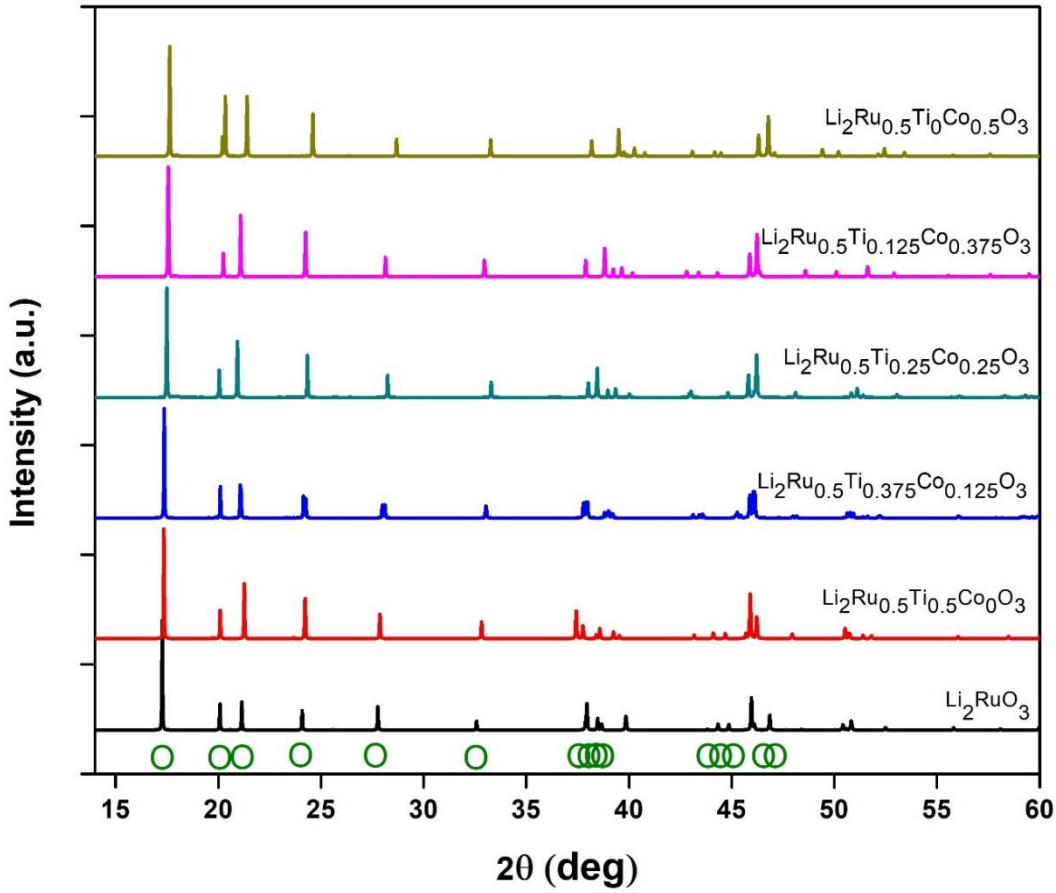

Figure 2: Simulated X-ray diffraction pattern of co-doped cathodes compared to that of the pristine Li_2RuO_3. The experimental data was shown in circles (green).

The calculated lattice parameters and volume changes are presented in Table 5. It can be seen from Table 5 that, lattice constant along *a*- and *b*- directions decreases while lattice constant along the *c*- axis increases after co-doping. Further, co-doping with Co, decreases the volume change when compared to Ti doped cathode. Smaller volume change in all doped cathodes indicate that there are no significant structural changes within the crystal structures which supports the analysis from X-ray diffraction pattern.

Table 5: Lattice constants, volumes and percentage volume changes ΔV(%) of cathodes

Cathode	***a*** **(Å)**	***b*****(Å)**	***c*****(Å)**	**Volume (Å^3)**	**ΔV (%)**
Li_2RuO_3	4.912	8.759	9.854	417.4	-
$Li_2Ru_{0.5}Ti_{0.5}Co_0O_3$	4.839	8.595	9.919	406.2	2.7
$Li_2Ru_{0.5}Ti_{0.375}Co_{0.125}O_3$	4.844	8.621	9.920	407.9	2.3
$Li_2Ru_{0.5}Ti_{0.25}Co_{0.25}O_3$	4.849	8.615	9.933	408.5	2.1
$Li_2Ru_{0.5}Ti_{0.125}Co_{0.375}O_3$	4.851	8.629	9.921	408.9	2.0
$Li_2Ru_{0.5}Ti_0Co_{0.5}O_3$	4.870	8.652	9.898	410.6	1.6

3.4. Thermodynamic stability

Thermodynamic stability is one of the important aspects which ensures that the battery will operate in a risk-free manner. Hence, it is necessary to study the thermodynamic stability of a cathode material before employing it in a battery. In LRO cathodes, removal of oxygen is thermodynamically more favorable than the oxidation of Ru. As a result, during the charging (extraction of Li-ions from the cathode) of the Li-ion battery, the LRO cathode decomposes via the following relation [45]:

$$Li_xRu_{0.5}Ti_yCo_{0.5-y}O_3\ (lattice) \rightarrow\ Li_xRu_{0.5}Ti_yCo_{0.5-y}O_{3-z}\ (lattice) + \frac{z}{2}O_2\ (gas) \qquad (3)$$

The thermodynamically favorable release of oxygen is one among the major problems in layered LRO cathodes. This is because, the thermodynamic stability of the cathode has direct correlation with the rate at which oxygen is released from the cathode. The carbon species coated on the electrode surfaces react with oxygen as it is released from the structure, affecting the formation of CO and CO_2 through an exothermic reaction. This reaction can destroy the cathode by causing an ignition or even explosion in the battery system. Therefore, the lifetime and electrochemical performance of LRO cathode materials can be enhanced significantly by controlling the oxygen loss and stabilizing oxygen inside the lattice itself.

To investigate the thermodynamic stability with regard to the oxygen evolution, Gibbs free energy (ΔG) has been calculated for the cathodes at various amounts (x) of Li by using the familiar equation $\Delta G = \Delta H - T\Delta S$, where ΔH is the change in enthalpy. ΔH for a cathode is calculated [46–48] using the following equation:

$$\Delta H(eV) = \frac{E(Li_xRu_{0.5}Ti_yCo_{0.5-y}O_{3-z}) + 0.5z\,E[O_2] - E(Li_xRu_{0.5}Ti_yCo_{0.5-y}O_3)}{0.5z} \qquad (4)$$

where, E is the total energy of the optimized crystal structure computed using the DFT+U method. The entropy change (ΔS) in equation (3), is nearly equal to the entropy of O_2, because O_2 is the only gas that is released. Accordingly, based on the earlier studies [48,49], the value of $T\Delta S$ is chosen as 0.63eV for O_2 molecule at standard temperature and pressure. Therefore, the Gibbs free energy (ΔG) of the LRO decomposition reaction (3) can be calculated as [48,50]:

$$\Delta G(eV) = \Delta H - 0.63 \qquad (5)$$

During the process of charging in a Li-ion battery, some electrons are removed from the cathode, which results in a decrease in the ΔG value of the reaction. At a given temperature, a decrease in the value of ΔG increases the rate at which oxygen is removed from the reaction mixture, which in turn causes the cathode to be destroyed more quickly. If the cathode structure breaks down more quickly, the temperature at which it decomposes will be lower. This will result in a lower reversible capacity, lower life time, and shrink in the range of safe operating conditions. If the value of ΔG is negative for a given amount of extracted lithium ions, the reaction will take place spontaneously.

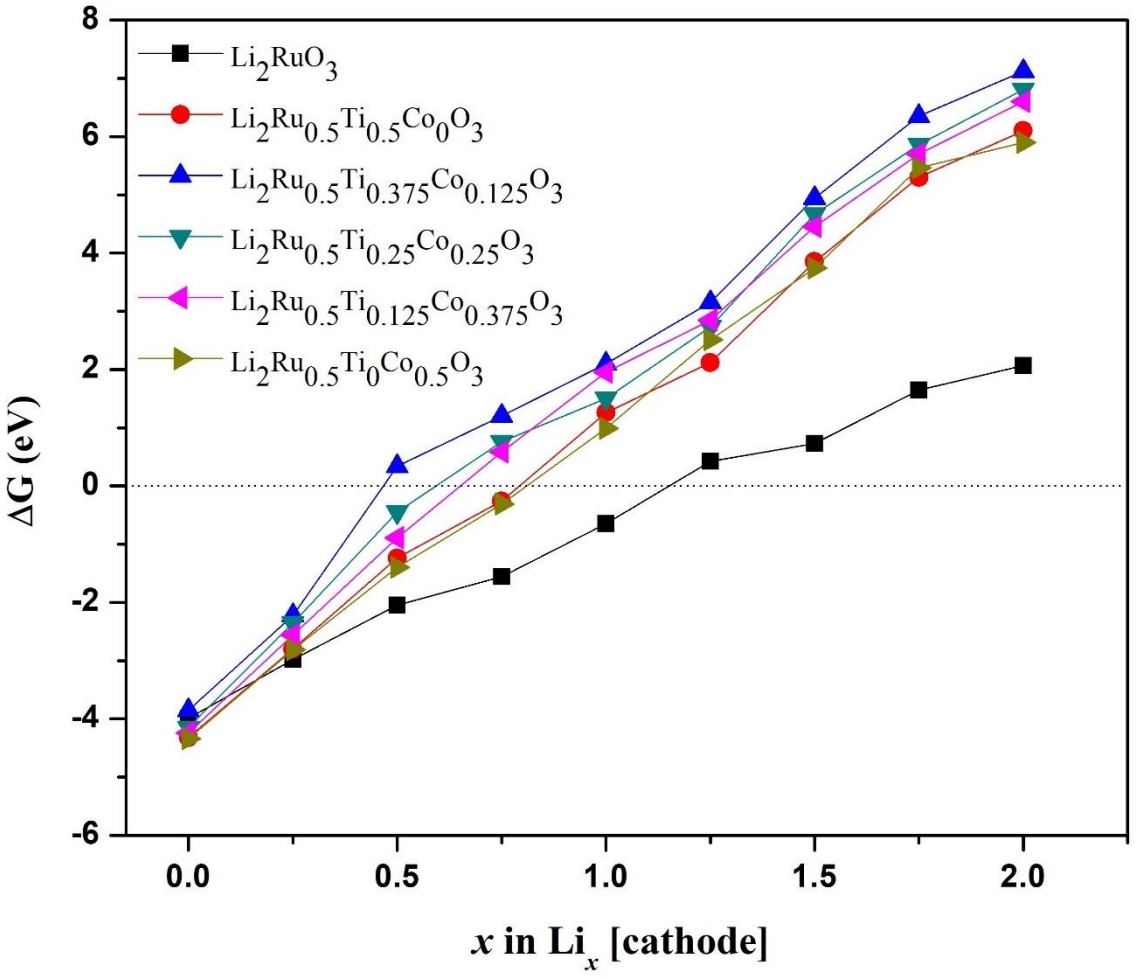

Figure 3: Calculated change in Gibb's free energy for the oxygen removal reaction at different Li-ion contents in the cathode materials.

Figure 3 depicts the calculated change in Gibbs free energy (ΔG) for the cathodes under consideration as a function of the amount of lithium extracted from the cathode. As seen in Figure 3, ΔG value for the LRO cathode turns negative when x in Li_x[cathode] reduced to 1.15, indicating that the spontaneous oxygen removal reaction occurs when $x \leq 1.15$. Similarly, for the co-doped cathodes $Li_2Ru_{0.5}Ti_{0.5}Co_0O_3$, $Li_2Ru_{0.5}Ti_{0.375}Co_{0.125}O_3$, $Li_2Ru_{0.5}Ti_{0.25}Co_{0.25}O_3$, $Li_2Ru_{0.5}Ti_{0.125}Co_{0.375}O_3$, and $Li_2Ru_{0.5}Ti_0Co_{0.5}O_3$, ΔG turns negative when $x \leq 0.79$, 0.47, 0.59, 0.65, and 0.81 respectively. The co-doped cathodes exhibit greater ΔG values when compared to the LRO cathode, which indicates that greater temperatures are required for the decomposition reaction to take place. Because of this, it is possible to draw the conclusion that all co-doped cathodes have a higher decomposition temperature compared to the unmodified LRO leading to higher reversible capacity and greater thermal stability of the co-doped cathodes. Among the studied co-doped cathodes, $Li_2Ru_{0.5}Ti_{0.375}Co_{0.125}O_3$ exhibits highest decomposition temperature and thermal stability. Based on these results, the order of thermal stability of the cathode structure is:

$Li_2Ru_{0.5}Ti_{0.375}Co_{0.125}O_3 > Li_2Ru_{0.5}Ti_{0.25}Co_{0.25}O_3 > Li_2Ru_{0.5}Ti_{0.125}Co_{0.375}O_3 > Li_2Ru_{0.5}Ti_{0.5}Co_0O_3 > Li_2Ru_{0.5}Ti_0Co_{0.5}O_3 > Li_2RuO_3$

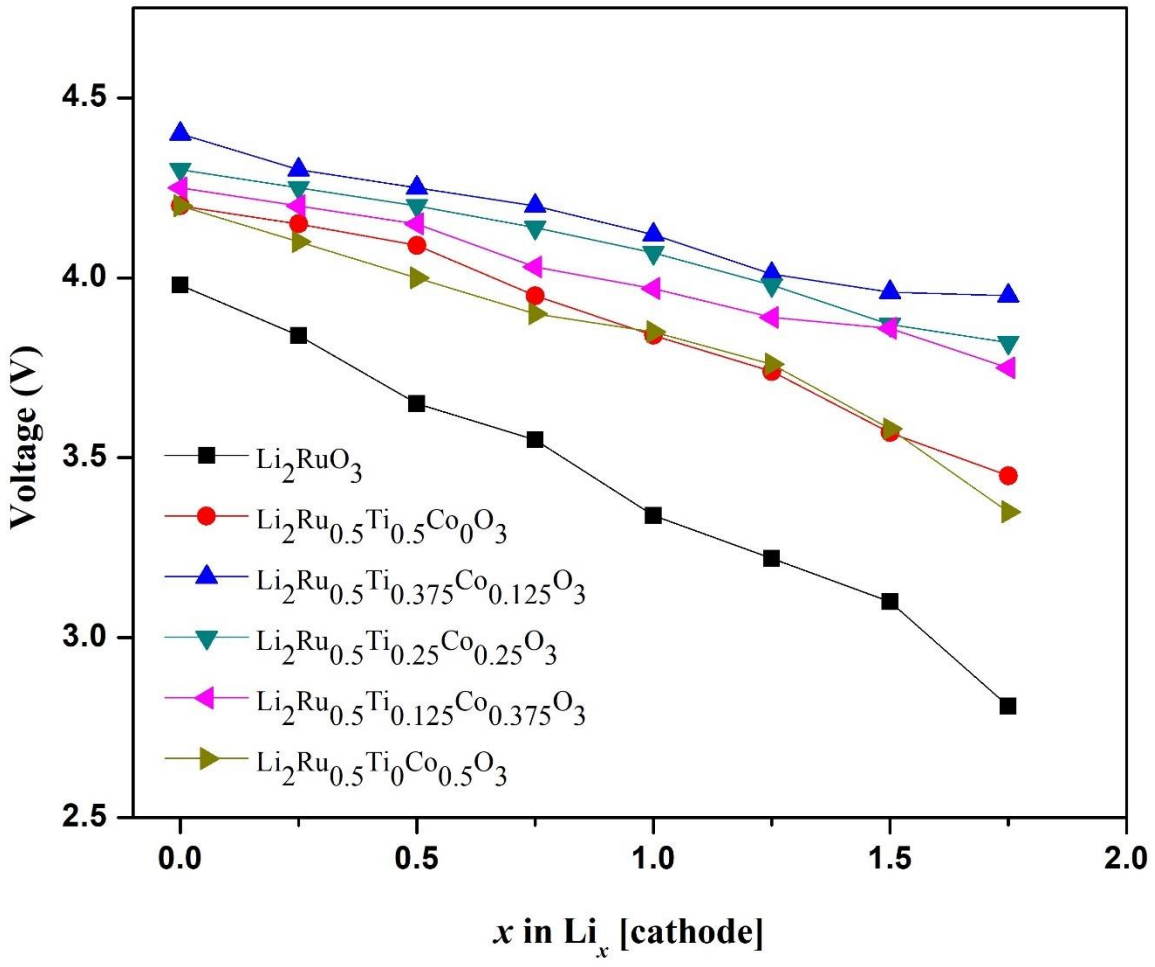

Figure 4: The calculated open circuit voltages of cathode materials at different Li-ion contents.

3.5. Voltage stability

The maximum power output a Lithium-ion battery is a function of the cell voltage, which in turn depends on the voltage of cathode and anode. LRO is a significant cathode material because of its ability to deliver a high open circuit voltage. However, the value of this voltage can change if dopants are introduced, and it is essential to have an understanding of the fluctuations in voltage that might occur as a result of the introduction of dopants. During the charge-discharge cycles, the following reaction takes place in the LIB when Li-solid is used as the anode:

$$Li_x[cathode] + (y - x)Li_{solid} \rightleftharpoons Li_y[cathode] \quad (6)$$

Here, x and y are Li-ions concentrations in the reactant and product states of the studied cathodes. As a result, the open-circuit voltage of the LIB at specific Li concentrations in the cathode can be computed by the following equation [51,52]:

$$V_{OC} = \frac{-\Delta\mu}{F} = \frac{\Delta E}{y-x} = \frac{E_{Li_y} - [E_{Li_x} + (y-x)E_{Li_{solid}}}{y-x} \quad (7)$$

where E is the total energy of the material calculated using DFT PBE+U potential of each electrode, μ is chemical potential (eV) and F is Faraday constant (C mol^{-1}).

Figure 4 shows the open-circuit voltages of co-doped cathode materials compared with the pristine LRO cathode. Maximum open-circuit voltage is possible when all the Li-ions are removed from the cathode. The maximum voltage for undoped LRO cathode is 3.98V whereas the maximum voltage of co-doped cathodes $Li_2Ru_{0.5}Ti_{0.5}Co_0O_3$, $Li_2Ru_{0.5}Ti_{0.375}Co_{0.125}O_3$, $Li_2Ru_{0.5}Ti_{0.25}Co_{0.25}O_3$, $Li_2Ru_{0.5}Ti_{0.125}Co_{0.375}O_3$, and $Li_2Ru_{0.5}Ti_0Co_{0.5}O_3$ is 4.2, 4.4, 4.3, 4.25, 4.2V respectively. The calculations show that using the co-doping strategy with Ti and Co increases the maximum voltage of pristine LRO at least by 5.5%. Among the co-doped cathodes, $Li_2Ru_{0.5}Ti_{0.375}Co_{0.125}O_3$ shows the highest maximum voltage (4.4V), which is about 10.5% higher than that of pristine LRO cathode. It has been observed that, at all Li concentrations in the cathode, the open circuit voltages of co-doped cathodes are higher than that of the pure LRO with $Li_2Ru_{0.5}Ti_{0.375}Co_{0.125}O_3$ exhibiting the highest voltage.

The voltage trend in Figure 4 can also be used to understand the voltage stability of cathodes. It is observed that, the voltage of the cathodes substantially decreases when the Li-ion content is changed from x = 0 to x = 1.8. Table 6 summarizes the voltage drop for each cathode as the content of Li-ions is increased from x = 0 to x = 1.8. The cut-off voltage is the lowest voltage at which a certain electronic device can function. The cut-off voltage is reached more quickly when the voltage reduction is larger. Because of this, the voltage stability decreases, which reduces the practical capacity. It is observed from Table 4, that all co-doped cathode materials experience less voltage reduction than the pristine LRO. More precisely, the voltage reduction of pristine LRO is 1.17V, while for the co-doped cathodes $Li_2Ru_{0.5}Ti_{0.5}Co_0O_3$, $Li_2Ru_{0.5}Ti_{0.375}Co_{0.125}O_3$, $Li_2Ru_{0.5}Ti_{0.25}Co_{0.25}O_3$, $Li_2Ru_{0.5}Ti_{0.125}Co_{0.375}O_3$, and $Li_2Ru_{0.5}Ti_0Co_{0.5}O_3$ is 0.75, 0.45, 0.48, 0.50, and 0.85V respectively. As a consequence, the co-doped cathodes have better voltage stability and practical capacity. In particular, $Li_2Ru_{0.5}Ti_{0.5}Co_0O_3$, $Li_2Ru_{0.5}Ti_{0.375}Co_{0.125}O_3$, $Li_2Ru_{0.5}Ti_{0.25}Co_{0.25}O_3$, $Li_2Ru_{0.5}Ti_{0.125}Co_{0.375}O_3$, and $Li_2Ru_{0.5}Ti_0Co_{0.5}O_3$ is 0.75, 0.45, 0.48, 0.50, and 0.85V respectively. The process of co-doping with Ti and Co significantly decreases the voltage drop at least by 44%, with maximum decrease achieved in $Li_2Ru_{0.5}Ti_{0.375}Co_{0.125}O_3$ (61%). These results show that co-doping with Ti and Co significantly increases the voltage stability and practical capacity of LRO cathode.

3.6. Electronic Structure

The total electronic density of states and partial density of states were calculated using DFT+U method. Figure 5 shows the total density of states (DOS) of each cathode. It is observed that bandgap does not exist at Fermi level of each cathode. However, bandgaps of cathodes are present in the conduction bands. To compare the bandgaps, energies of each cathode are shifted by the corresponding Fermi level. The bandgaps extracted from the DOS structure are presented in Table 7.

The partial density of states (PDOS) of cathode materials were calculated using DFT+U method and presented in Figure 6. It is observed that in all samples, the majority of the valence band electronic states are created by the 2p orbitals of O atoms, even though the valence band itself contains both oxygen and transition metals. In contrast, all six compounds show a greater metallic contribution in the conduction band, suggesting that the transition metal is primarily responsible for the conductivity of the cathode materials. It is also observed from the PDOS structure that there is a strong hybridization between oxygen and transition metal (TM) orbitals implying a strong TM-O bonding and greater oxygen stability in the cathode materials.

Table 6: The voltage reduction values of the studied cathode materials extracted from the open circuit voltage plots in Figure 4.

Cathode	Voltage Reduction (V)
Li_2RuO_3	1.17
$Li_2Ru_{0.5}Ti_{0.5}Co_0O_3$	0.75
$Li_2Ru_{0.5}Ti_{0.375}Co_{0.125}O_3$	0.45
$Li_2Ru_{0.5}Ti_{0.25}Co_{0.25}O_3$	0.48
$Li_2Ru_{0.5}Ti_{0.125}Co_{0.375}O_3$	0.50
$Li_2Ru_{0.5}Ti_0Co_{0.5}O_3$	0.85

To verify the bandgaps extracted from the electronic density of states, we have calculated the optical absorption spectra of cathode materials. Figure 7 shows the optical absorption spectra of pristine and co-doped cathode materials. The bandgaps extracted from the optical absorption spectra are compared with those obtained from the DOS structure in Table 7. It can be seen from Table 7 that, bandgaps of cathode materials obtained by two methods are strongly correlated implying that the electronic structure calculations are accurate.

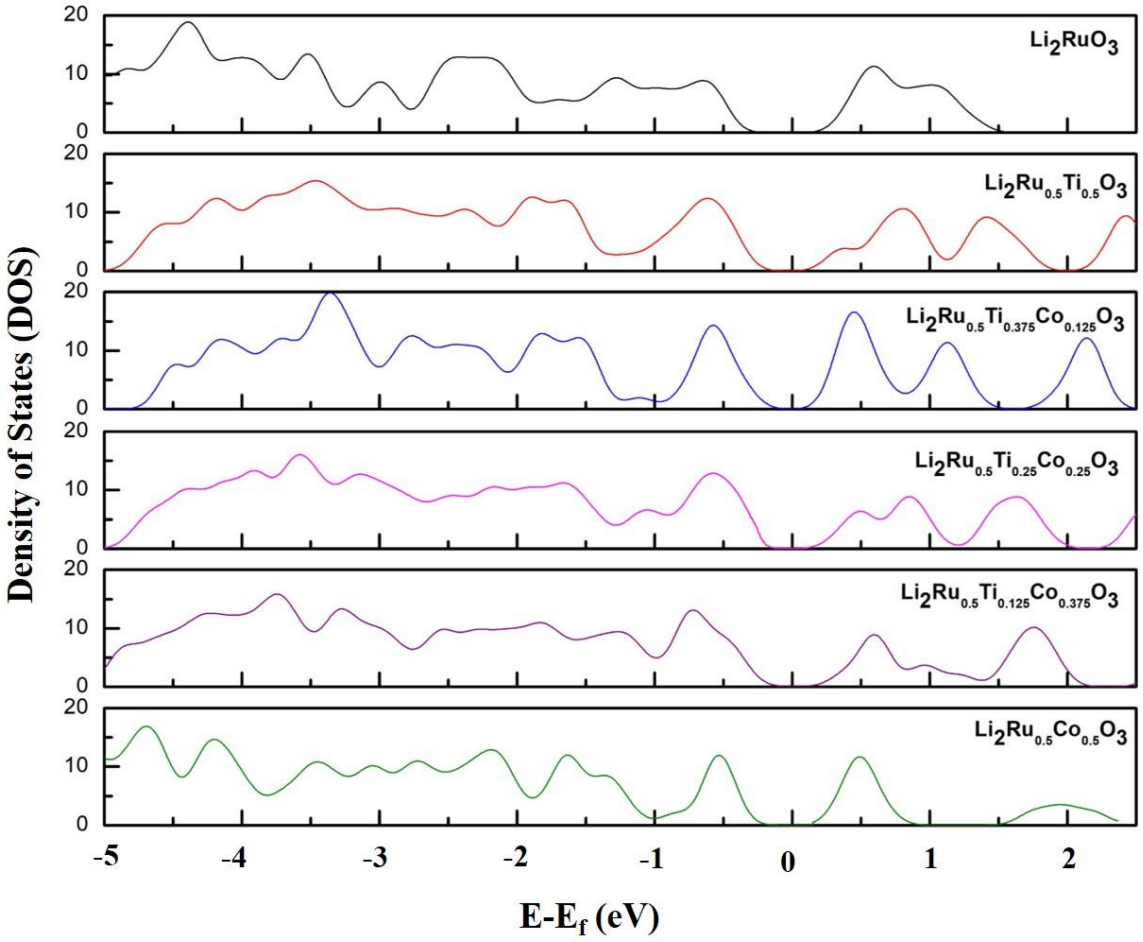

Figure 5: Density of States (DOS) of pristine and co-doped cathodes

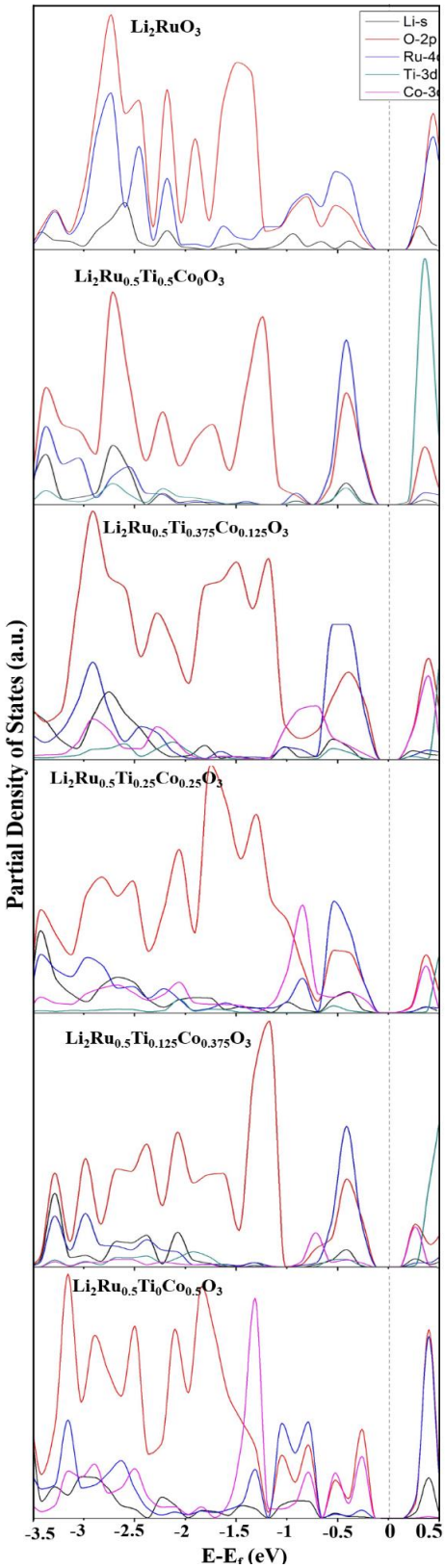

Figure 6: Partial Density of States (PDOS) of pristine and co-doped cathodes

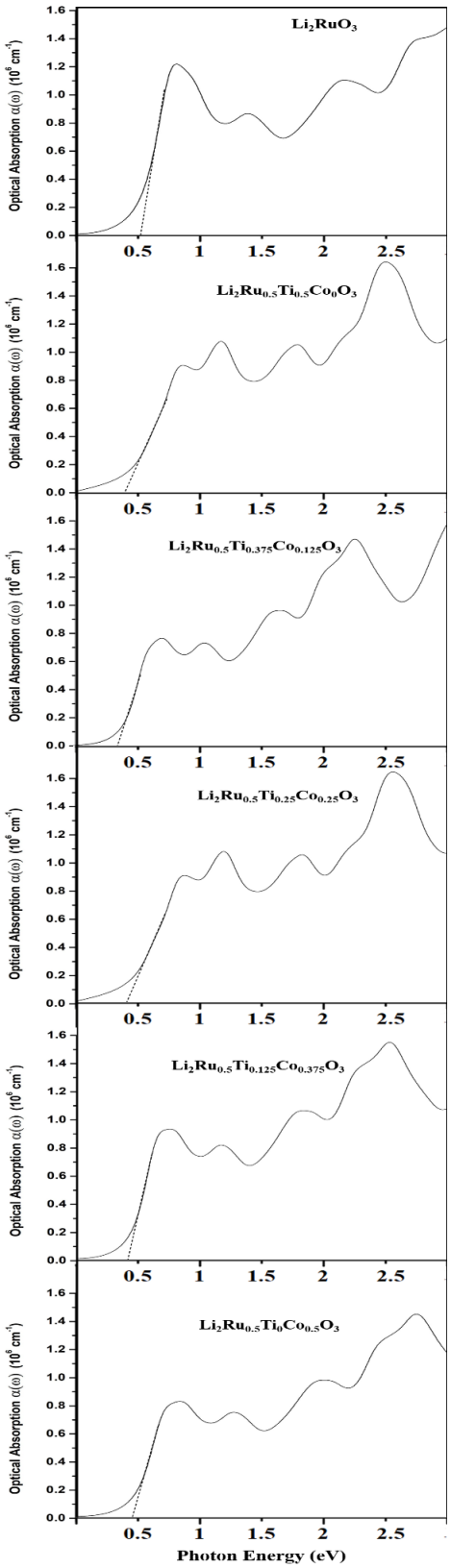

Figure 7: Optical absorption spectra of pristine and co-doped cathodes

Table 7: The bandgaps of the studied cathode materials calculated from electronic DOS, optical absorption spectra and percentage change in the bandgap when compared to the pristine Li_2RuO_3.

Cathode	Bandgap (eV) from DOS and percentage change	Bandgap (eV) from Optical absorption
Li_2RuO_3	0.51	0.52
$Li_2Ru_{0.5}Ti_{0.5}Co_0O_3$	0.41 (18%)	0.41
$Li_2Ru_{0.5}Ti_{0.375}Co_{0.125}O_3$	0.30 (40%)	0.32
$Li_2Ru_{0.5}Ti_{0.25}Co_{0.25}O_3$	0.38 (24%)	0.39
$Li_2Ru_{0.5}Ti_{0.125}Co_{0.375}O_3$	0.40 (20%)	0.42
$Li_2Ru_{0.5}Ti_0Co_{0.5}O_3$	0.47 (6%)	0.46

Table 7 summarizes the bandgaps of pristine LRO, and co-doped LRO cathodes obtained from electronic DOS structure and optical absorption spectra. From Table 7, the electronic band gap of undoped LRO is 0.51eV which is in good agreement with the findings of other researches [53,54]. The electronic bandgaps of co-doped cathodes are 0.41, 0.30, 0.38, 0.40, and 0.47 for $Li_2Ru_{0.5}Ti_{0.5}Co_0O_3$, $Li_2Ru_{0.5}Ti_{0.375}Co_{0.125}O_3$, $Li_2Ru_{0.5}Ti_{0.25}Co_{0.25}O_3$, $Li_2Ru_{0.5}Ti_{0.125}Co_{0.375}O_3$, and $Li_2Ru_{0.5}Ti_0Co_{0.5}O_3$ respectively. The bandgaps obtained from the optical absorption spectra agree well with the DOS bandgaps implying that the results of electronic structure calculations are accurate. These results show that co-doping with Ti and Co decreases the bandgap at least by 6%. The dopants generate impurity states and facilitates the electronic transfer to the conduction band. Electrical conductivity is inversely proportional to the value of bandgap, the pristine LRO is expected to have lowest electrical conductivity among the studies cathodes. Further, the electrical conductivity of the LRO cathode increases significantly with co-doping strategy. Based on the values of bandgap, the increasing order of electrical conductivity of studied cathodes is expected to be as follows:

$Li_2Ru_{0.5}Ti_{0.375}Co_{0.125}O_3 < Li_2Ru_{0.5}Ti_{0.25}Co_{0.25}O_3 < Li_2Ru_{0.5}Ti_{0.125}Co_{0.375}O_3 < Li_2Ru_{0.5}Ti_{0.5}Co_0O_3 < Li_2Ru_{0.5}Ti_0Co_{0.5}O_3 < Li_2RuO_3$

Conclusions

In this work, the effect of co-doping with transition metals Ti and Co on various parameters that determine the electrochemical properties of Li_2RuO_3 were investigated using the DFT+U quantum mechanical calculations. The key findings of this study are summarized below:

1. Co-doping with Ti and Co improves the theoretical charge capacity of Li_2RuO_3 by at least 14.9% and $Li_2Ru_{0.5}Ti_{0.5}Co_0O_3$ has the highest capacity.
2. Formation energy of co-doped cathodes is higher than that of pristine Li_2RuO_3 by at least 18.4% with $Li_2Ru_{0.5}Ti_{0.375}Co_{0.125}O_3$ showing the highest formation energy of -14.81eV.
3. Co-doping with Ti and Co does not lead to appreciable crystal structural changes.
4. Co-doping with Ti and Co reduces oxygen evolution from the cathode and all co-doped cathodes have higher decomposition temperatures compared to the pristine Li_2RuO_3 leading to higher reversible capacity and greater thermal stability. The cathode $Li_2Ru_{0.5}Ti_{0.375}Co_{0.125}O_3$ exhibits highest thermal stability.

5. Co-doping with Ti and Co increases the maximum voltage of pristine LRO at least by 5.5%. Among the co-doped cathodes, $Li_2Ru_{0.5}Ti_{0.375}Co_{0.125}O_3$ shows the highest maximum voltage (4.4V), which is about 10.5% higher than that of pristine LRO cathode.
6. The process of co-doping with Ti and Co significantly decreases the voltage reduction at least by 44%, with maximum decrease achieved in $Li_2Ru_{0.5}Ti_{0.375}Co_{0.125}O_3$ (61%).
7. Co-doping with Ti and Co decreases the bandgap at least by 6%. Bandgaps obtained from the electronic DOS are in good agreement with those obtained from the optical absorption spectra supporting the validity of electronic structure calculations.

Acknowledgements

One of the authors C. Bapanayya greatly acknowledges Dr. M. Sreekanth and Dr. N. Parvathala Reddy for their suggestions and discussions during the progress of the research work and development of the manuscript.

References

[1] L. Lu, X. Han, J. Li, J. Hua, M. Ouyang, A review on the key issues for lithium-ion battery management in electric vehicles, J. Power Sources. 226 (2013) 272–288. https://doi.org/10.1016/J.JPOWSOUR.2012.10.060.

[2] M. Xu, Z. Chen, H. Zhu, X. Yan, L. Li, Q. Zhao, Mitigating capacity fade by constructing highly ordered mesoporous Al_2O_3/polyacene double-shelled architecture in Li-rich cathode materials, J. Mater. Chem. A. 3 (2015) 13933–13945. https://doi.org/10.1039/C5TA03676C.

[3] D. Ye, B. Wang, Y. Chen, G. Han, Z. Zhang, D. Hulicova-Jurcakova, J. Zou, L. Wang, Understanding the stepwise capacity increase of high energy low-Co Li-rich cathode materials for lithium ion batteries, J. Mater. Chem. A. 2 (2014) 18767–18774. https://doi.org/10.1039/C4TA03692A.

[4] M.M. Kalantarian, S. Asgari, P. Mustarelli, Theoretical investigation of Li_2MnSiO_4 as a cathode material for Li-ion batteries: a DFT study, J. Mater. Chem. A. 1 (2013) 2847–2855. https://doi.org/10.1039/C2TA01363K.

[5] B. Song, T. Sui, S. Ying, L. Li, L. Lu, A.M. Korsunsky, Nano-structural changes in Li-ion battery cathodes during cycling revealed by FIB-SEM serial sectioning tomography, J. Mater. Chem. A. 3 (2015) 18171–18179. https://doi.org/10.1039/C5TA04151A.

[6] Q. Li, G. Li, C. Fu, D. Luo, J. Fan, D. Xie, L. Li, Balancing stability and specific energy in Li-rich cathodes for lithium ion batteries: a case study of a novel Li–Mn–Ni–Co oxide, J. Mater. Chem. A. 3 (2015) 10592–10602. https://doi.org/10.1039/C5TA00929D.

[7] K. Mizushima, P.C. Jones, P.J. Wiseman, J.B. Goodenough, $LixCoO_2$ ($0<x\leq1$): A new cathode material for batteries of high energy density, Solid State Ionics. 3–4 (1981) 171–174. https://doi.org/10.1016/0167-2738(81)90077-1.

[8] A.K. Padhi, Phospho-olivines as Positive-Electrode Materials for Rechargeable Lithium Batteries, J. Electrochem. Soc. 144 (1997) 1188. https://doi.org/10.1149/1.1837571.

[9] S. Liu, J. Wang, Z. Tian, Q. Li, X. Tian, Y. Cui, Y. Yang, Chromium doped Li2RuO3 as a positive electrode with superior electrochemical performance for lithium ion batteries, Chem. Commun. 53 (2017) 11913–11916. https://doi.org/10.1039/C7CC07545F.

[10] A. Lanjan, B. Ghalami Choobar, S. Amjad-Iranagh, First principle study on the

application of crystalline cathodes $Li_2Mn_{0.5}TM_{0.5}O_3$ for promoting the performance of lithium-ion batteries, Comput. Mater. Sci. 173 (2020) 109417. https://doi.org/https://doi.org/10.1016/j.commatsci.2019.109417.

[11] J. Wang, Y. Zhao, X. Zhang, H. Wu, S. Hu, K. Wei, Y. Cui, W. Su, Y. Cui, Trace molybdenum doped Li_2RuO_3 as a cathode material with enhanced performance for lithium ion batteries, Sustain. Energy Fuels. 3 (2019) 2697–2704. https://doi.org/10.1039/C9SE00370C.

[12] M. Lengyel, K.-Y. Shen, D.M. Lanigan, J.M. Martin, X. Zhang, R.L. Axelbaum, Trace level doping of lithium-rich cathode materials, J. Mater. Chem. A. 4 (2016) 3538–3545. https://doi.org/10.1039/C5TA07764H.

[13] F. Wu, W. Li, L. Chen, Y. Su, L. Bao, W. Bao, Z. Yang, J. Wang, Y. Lu, S. Chen, Renovating the electrode-electrolyte interphase for layered lithium- & manganese-rich oxides, Energy Storage Mater. 28 (2020) 383–392. https://doi.org/https://doi.org/10.1016/j.ensm.2019.12.017.

[14] Y. Su, F. Yuan, L. Chen, Y. Lu, J. Dong, Y. Fang, S. Chen, F. Wu, Enhanced high-temperature performance of Li-rich layered oxide via surface heterophase coating, J. Energy Chem. 51 (2020) 39–47. https://doi.org/https://doi.org/10.1016/j.jechem.2020.03.033.

[15] W. Yin, A. Grimaud, G. Rousse, A.M. Abakumov, A. Senyshyn, L. Zhang, S. Trabesinger, A. Iadecola, D. Foix, D. Giaume, J.-M. Tarascon, Structural evolution at the oxidative and reductive limits in the first electrochemical cycle of $Li_{1.2}Ni_{0.13}Mn_{0.54}Co_{0.13}O_2$, Nat. Commun. 11 (2020) 1252. https://doi.org/10.1038/s41467-020-14927-4.

[16] M.-S. Park, Y.-G. Lim, J.-W. Park, J.-S. Kim, J.-W. Lee, J.H. Kim, S.X. Dou, Y.-J. Kim, Li_2RuO_3 as an Additive for High-Energy Lithium-Ion Capacitors, J. Phys. Chem. C. 117 (2013) 11471–11478. https://doi.org/10.1021/jp4005828.

[17] S. Zheng, F. Zheng, H. Liu, G. Zhong, J. Wu, M. Feng, Q. Wu, W. Zuo, C. Hong, Y. Chen, K. An, P. Liu, S. Wu, Y. Yang, Novel Ordered Rocksalt-Type Lithium-Rich $Li_2Ru_{1-x}Ni_xO_{3-\delta}$ $(0.3 \leq x \leq 0.5)$ Cathode Material with Tunable Anionic Redox Potential, ACS Appl. Energy Mater. 2 (2019) 5933–5944. https://doi.org/10.1021/acsaem.9b01051.

[18] P. Arunkumar, W.J. Jeong, S. Won, W. Bin Im, Improved electrochemical reversibility of over-lithiated layered Li_2RuO_3 cathodes: Understanding aliovalent Co3+ substitution with excess lithium, J. Power Sources. 324 (2016) 428–438. https://doi.org/10.1016/j.jpowsour.2016.05.013.

[19] A.K. Kalathil, P. Arunkumar, D.H. Kim, J.-W. Lee, W. Bin Im, Influence of Ti^{4+} on the Electrochemical Performance of Li-Rich Layered Oxides - High Power and Long Cycle Life of $Li_2Ru_{1-x}Ti_xO_3$ Cathodes, ACS Appl. Mater. Interfaces. 7 (2015) 7118–7128. https://doi.org/10.1021/am507951x.

[20] F.P. Nkosi, K. Raju, N. Palaniyandy, M. V Reddy, C. Billing, K.I. Ozoemena, Insights into the Synergistic Roles of Microwave and Fluorination Treatments towards Enhancing the Cycling Stability of P2-Type $Na_{0.67}[Mg_{0.28}Mn_{0.72}]O_2$ Cathode Material for Sodium-Ion Batteries, J. Electrochem. Soc. 164 (2017) A3362–A3370. https://doi.org/10.1149/2.1721713jes.

[21] L. Torres-Castro, M.A. Abreu-Sepulveda, R.S. Katiyar, A. Manivannan, Electrochemical Investigations on the Effect of Mg-Substitution in Li_2MnO_3 Cathode,

J. Electrochem. Soc. 164 (2017) A1464–A1473. https://doi.org/10.1149/2.0661707jes.

[22] J. Duan, G. Hu, Y. Cao, K. Du, Z. Peng, Synthesis of high-performance Fe–Mg-co-doped $LiMnPO_4$/C via a mechano-chemical liquid-phase activation technique, Ionics (Kiel). 22 (2016) 609–619. https://doi.org/10.1007/s11581-015-1582-0.

[23] D. Aasen, M.P. Clark, D.G. Ivey, Investigation of Transition Metal-Based (Mn, Co, Ni, Fe) Trimetallic Oxide Nanoparticles on N-doped Carbon Nanotubes as Bifunctional Catalysts for Zn-Air Batteries, J. Electrochem. Soc. 167 (2020) 40503. https://doi.org/10.1149/1945-7111/ab7094.

[24] Y. Zhang, H. Fan, M. Han, Stability of Ni-YSZ Anode for SOFCs in Methane Fuel: The Effects of Infiltrating $La_{0.8}Sr_{0.2}FeO_3$ and Gd-Doped CeO_2Materials, J. Electrochem. Soc. 165 (2018) F756–F763. https://doi.org/10.1149/2.0171810jes.

[25] S. Pang, M. Zhu, K. Xu, X. Shen, H. Wen, Y. Su, G. Yang, X. Wu, S. Li, W. Wang, X. Xi, H. Wang, Enhanced Electrochemical Performance of $Li_{1.2}Mn_{0.54}Ni_{0.13}Co_{0.13}O_2$ via L-Ascorbic Acid-Based Treatment as Cathode Material for Li-Ion Batteries, J. Electrochem. Soc. 165 (2018) A1897–A1902. https://doi.org/10.1149/2.1481809jes.

[26] S. Yanxia, H. Chunxi, S. Yue, Z. Jinbo, Z. Lijuan, L. Xiang, R. Xiufeng, D. Shengde, Z. Guotai, S. Chao, Z. Yuan, Improved Lithium Ion Diffusion and Stability of a $LiNi_{0.8}Co_{0.1}Mn_{0.1}O_2$ Cathode via the Synergistic Effect of Na and Mg Dual-Metal Cations for Lithium Ion Battery, J. Electrochem. Soc. 167 (2020) 20522. https://doi.org/10.1149/1945-7111/ab6977.

[27] X. He, G. Han, S. Lou, L. Du, X. Xu, C. Du, X. Cheng, P. Zuo, Y. Ma, H. Huo, G. Yin, Improved Electrochemical Performance of $LiNi_{0.8}Co_{0.15}Al_{0.05}O_2$ Cathode Material by Coating of Graphene Nanodots, J. Electrochem. Soc. 166 (2019) A1038–A1044. https://doi.org/10.1149/2.0541906jes.

[28] J.P. Perdew, K. Burke, M. Ernzerhof, Generalized gradient approximation made simple, Phys. Rev. Lett. 77 (1996) 3865–3868. https://doi.org/10.1103/PhysRevLett.77.3865.

[29] R.R. Neelakantaiah, B.B. Dasari, P.M. Ette, K. Ramesha, Improving the Electrochemical Performance of Li_2RuO_3 through Chemical Substitution: A Case Study of (x)$LiCoO_2$-(1-x)Li_2RuO_3 Solid Solution (x≤0.4), ChemElectroChem. 7 (2020) 328–335. https://doi.org/10.1002/celc.201902059.

[30] S. Chen, J. Lin, Q. Shi, Z. Cai, L. Cao, L. Zhu, Z. Yuan, Nanoscale Iron Fluoride Supported by Three-Dimensional Porous Graphene as Long-Life Cathodes for Lithium-Ion Batteries, J. Electrochem. Soc. 167 (2020) 80506. https://doi.org/10.1149/1945-7111/ab88be.

[31] H.R. Jiang, T.S. Zhao, L. Shi, P. Tan, L. An, First-Principles Study of Nitrogen-, Boron-Doped Graphene and Co-Doped Graphene as the Potential Catalysts in Nonaqueous Li–O_2 Batteries, J. Phys. Chem. C. 120 (2016) 6612–6618. https://doi.org/10.1021/acs.jpcc.6b00136.

[32] X. Tian, S. Liu, X. Jiang, F. Ye, R. Cai, A new lithium-rich layer-structured cathode material with improved electrochemical performance and voltage maintenance, Int. J. Energy Res. 43 (2019) 7547–7556. https://doi.org/https://doi.org/10.1002/er.4724.

[33] Z. Moradi, A. Lanjan, S. Srinivasan, Enhancement of Electrochemical Properties of Lithium Rich Li_2RuO_3 Cathode Material , J. Electrochem. Soc. 167 (2020). https://doi.org/10.1149/1945-7111/aba44d.

[34] Z. Moradi, A. Lanjan, S. Srinivasan, Multiscale Investigation into the Co-Doping Strategy on the Electrochemical Properties of Li_2RuO_3 Cathodes for Li-Ion Batteries,

ChemElectroChem. 8 (2021) 112–124. https://doi.org/https://doi.org/10.1002/celc.202001206.
[35] J.M. Tarascon, M. Armand, Issues and challenges facing rechargeable lithium batteries, Nature. (2001). https://doi.org/10.1038/35104644.
[36] V.I. Anisimov, F. Aryasetiawan, A.I. Lichtenstein, First-principles calculations of the electronic structure and spectra of strongly correlated systems: the LDA-U method, J. Phys. Condens. Matter. 9 (1997) 767–808. https://doi.org/10.1088/0953-8984/9/4/002.
[37] J.P. Perdew, K. Burke, M. Ernzerhof, Generalized Gradient Approximation Made Simple, Phys. Rev. Lett. 77 (1996) 3865–3868. https://doi.org/10.1103/PhysRevLett.77.3865.
[38] A. Lanjan, B. Ghalami Choobar, S. Amjad-Iranagh, Promoting lithium-ion battery performance by application of crystalline cathodes $Li_xMn_{1-z}Fe_zPO_4$, J. Solid State Electrochem. 24 (2020) 157–171. https://doi.org/10.1007/s10008-019-04480-6.
[39] F. Aryasetiawan, K. Karlsson, O. Jepsen, U. Schönberger, Calculations of Hubbard -U from first-principles, Phys. Rev. B. 74 (2006) 125106. https://doi.org/10.1103/PhysRevB.74.125106.
[40] Y. Gao, X. Wang, J. Ma, Z. Wang, L. Chen, Selecting Substituent Elements for Li-Rich Mn-Based Cathode Materials by Density Functional Theory (DFT) Calculations, Chem. Mater. 27 (2015) 3456–3461. https://doi.org/10.1021/acs.chemmater.5b00875.
[41] B. Farkaš, D. Santos-Carballal, A. Cadi-Essadek, N.H. de Leeuw, A DFT+U study of the oxidation of cobalt nanoparticles: Implications for biomedical applications, Materialia. 7 (2019) 100381. https://doi.org/https://doi.org/10.1016/j.mtla.2019.100381.
[42] A.C.W.P. James, J.B. Goodenough, Structure and bonding in lithium ruthenate, Li_2RuO_3, J. Solid State Chem. 74 (1988) 287–294. https://doi.org/10.1016/0022-4596(88)90357-X.
[43] K. Momma, F. Izumi, VESTA 3 for three-dimensional visualization of crystal, volumetric and morphology data, J. Appl. Crystallogr. 44 (2011) 1272–1276. https://doi.org/10.1107/S0021889811038970.
[44] M. Zhi, C. Xiang, J. Li, M. Li, N. Wu, Nanostructured carbon–metal oxide composite electrodes for supercapacitors: a review, Nanoscale. 5 (2013) 72–88. https://doi.org/10.1039/C2NR32040A.
[45] P. Xiao, Z.Q. Deng, A. Manthiram, G. Henkelman, Calculations of Oxygen Stability in Lithium-Rich Layered Cathodes, J. Phys. Chem. C. 116 (2012) 23201–23204. https://doi.org/10.1021/jp3058788.
[46] M.Y. Yang, S. Kim, K. Kim, W. Cho, J.W. Choi, Y.S. Nam, Role of Ordered Ni Atoms in Li Layers for Li-Rich Layered Cathode Materials, Adv. Funct. Mater. 27 (2017) 1700982. https://doi.org/https://doi.org/10.1002/adfm.201700982.
[47] S. Wang, J. Liu, Q. Sun, New allotropes of Li_2MnO_3 as cathode materials with better cycling performance predicted in high pressure synthesis, J. Mater. Chem. A. 5 (2017) 16936–16943. https://doi.org/10.1039/C7TA04941B.
[48] H. Zhang, Y. Gong, J. Li, K. Du, Y. Cao, J. Li, Selecting substituent elements for $LiMnPO_4$ cathode materials combined with density functional theory (DFT) calculations and experiments, J. Alloys Compd. 793 (2019) 360–368. https://doi.org/https://doi.org/10.1016/j.jallcom.2019.04.191.
[49] S. Francis Amalraj, B. Markovsky, D. Sharon, M. Talianker, E. Zinigrad, R. Persky, O.

Haik, J. Grinblat, J. Lampert, M. Schulz-Dobrick, A. Garsuch, L. Burlaka, D. Aurbach, Study of the electrochemical behavior of the "inactive" Li_2MnO_3, Electrochim. Acta. 78 (2012) 32–39. https://doi.org/https://doi.org/10.1016/j.electacta.2012.05.144.

[50] F. Zheng, S. Zheng, P. Zhang, X. Zhang, S. Wu, Y. Yang, Z.Z. Zhu, Impact of Structural Transformation on Electrochemical Performances of Li-Rich Cathode Materials: The Case of Li_2RuO_3, J. Phys. Chem. C. 123 (2019) 13491–13499. https://doi.org/10.1021/acs.jpcc.9b02887.

[51] J.B. Goodenough, K.S. Park, The Li-ion rechargeable battery: A perspective, J. Am. Chem. Soc. (2013). https://doi.org/10.1021/ja3091438.

[52] B. Medasani, A. Gamst, H. Ding, W. Chen, K.A. Persson, M. Asta, A. Canning, M. Haranczyk, Predicting defect behavior in B2 intermetallics by merging ab initio modeling and machine learning, Npj Comput. Mater. 2 (2016) 1. https://doi.org/10.1038/s41524-016-0001-z.

[53] M.D. Johannes, A.M. Stux, K.E. Swider-Lyons, Electronic structure and properties of Li-insertion materials: Li_2RuO_3 and RuO_2, Phys. Rev. B. 77 (2008) 75124. https://doi.org/10.1103/PhysRevB.77.075124.

[54] Z. V Pchelkina, A.L. Pitman, A. Moewes, E.Z. Kurmaev, T.-Y. Tan, D.C. Peets, J.-G. Park, S. V Streltsov, Electronic structure of Li_2RuO_3 studied by LDA and LDA+DMFT calculations and soft x-ray spectroscopy, Phys. Rev. B. 91 (2015) 115138. https://doi.org/10.1103/PhysRevB.91.115138.